Growth and sintering of Pd clusters on α-Al_2O_3(0001)

Steven L. Tait
Department of Physics, University of Washington, Seattle, Washington 98195-1560

Lien T. Ngo
Department of Chemistry, University of Washington, Seattle, Washington 98195-1700

Qiuming Yu and Samuel C. Fain, Jr.
Department of Physics, University of Washington, Seattle, Washington 98195-1560

Charles T. Campbell[a)]
Department of Chemistry, University of Washington, Seattle, Washington 98195-1700

(Received 27 August 2004; accepted 23 November 2004; published online 3 February 2005)

The growth and sintering of Pd nanoparticles on α-Al_2O_3(0001) have been studied by noncontact atomic force microscopy (NC-AFM), low-energy ion scattering spectroscopy (LEIS), temperature-programmed desorption (TPD) and x-ray photoelectron spectroscopy (XPS). This is the first study of metal nanoparticles on a well-defined oxide surface where both NC-AFM and LEIS are used for characterization. These prove to be a powerful combination in assessing particle dimensions. The clean alumina surface showed atomically flat, 200–700 nm wide terraces. The sharp step edges are straight (within our resolution) for lengths of >300 nm and have heights in multiples of 0.2 nm. The Pd grows initially as two-dimensional (2D) islands at 300 K, with the transition to 3D particle growth at 0.25 ML (ML=monolayers). Upon heating at 1 K/s, the Pd starts to sinter below 400 K, and sinters at a nearly constant rate with increasing temperature, covering ~50% less of the alumina surface by ~1000 K, with a doubling in particle diameter and an eightfold decrease in particle number density. By ~1000 K, the number density was $\sim 9 \times 10^{11}/cm^2$ for 0.8 ML of Pd, with an average diameter of 5 nm and an average thickness of 1 nm. © *2005 American Institute of Physics*. [DOI: 10.1063/1.1849151]

I. INTRODUCTION

Many catalysts for energy and/or environmental technology consist of transition metal nanoparticles immobilized on oxide supports. The activity and selectivity of these catalysts depend on metal particle size, and the increase in average particle size with time (i.e., sintering) is a major industrial problem. To fundamentally understand these phenomena, many researchers have adopted a model catalyst approach whereby metal nanoparticles are supported on a single-crystalline oxide surface. This allows for easier measurement and control of the cleanliness, size, number density, and shape of the particles. Often, the oxide is in the form of an ultrathin film grown on a metallic crystal, which allows scanning tunneling microscopy (STM) to be used to characterize the nanoparticles, even with insulating oxides. However, it is often found that the supported metal diffuses through the oxide and reacts with the underlying metallic crystal, which complicates sintering and reactivity studies. In these cases, it is preferable to use a bulk single crystal of the oxide for these model catalysts, which however precludes use of STM if the oxide is an insulator, as is alumina. Thus, one is forced to use atomic force microscopy (AFM) instead of STM, resulting in limitations of spatial resolution. Few AFM studies of clean metal nanoparticles on single-crystalline, insulator oxide surfaces have been reported. To our knowledge, there have been no previous studies of this type in which the surface structure was also characterized with a technique such as low-energy ion scattering spectroscopy (LEIS) which probes only the topmost atomic layer of the solid. Here, we apply NC-AFM (NC—noncontact) and LEIS to study the growth and sintering of Pd nanoparticles on α-Al_2O_3(0001), and prove this to be a very powerful combination for such studies. Structural information from LEIS helps to overcome problems in measuring small particle sizes inherent to NC-AFM.

Palladium nanoclusters supported on alumina are catalysts for cleaner methane combustion, an industrially important reaction that reduces NO_x emissions. These catalysts thus have been the subject of much study from both a practical and fundamental point of view.[1–10] This catalyst would find much broader application if its long-term deactivation by sintering could be prevented. Fundamental studies of its sintering kinetics may yield ideas on how to prevent or slow the sintering of this and other oxide-supported metal nanoparticle catalysts. Also, a more complete understanding of the sintering kinetics may lead to better short-term screening tests for predicting the long-term stability of new catalysts, and thus accelerate their development.

In this paper, we present results of growth and sintering studies of Pd clusters on α-alumina, using temperature-programmed low-energy ion scattering (TP-LEIS) and NC-AFM. TP-LEIS samples only the top layer of the surface and is an ideal technique for determining the percentage of oxide

[a)]Author to whom correspondence should be addressed; FAX: (206) 616-6250; Electronic mail: campbell@chem.washington.edu

surface covered by the metal. NC-AFM yields topography information about the sample surface, providing local cluster size and number density data. Ultimately we plan to simulate the sintering kinetics measured here with a new general model for sintering kinetics presented previously,[11] to test the validity of that new model.

There have been beautiful STM studies of Pd particles on highly ordered thin films of Al_2O_3 grown on NiAl(110) which provided superb measurements of particle size distributions and number densities, even achieving atomic resolution on the particles.[12] However, these thin-film samples are unsuitable for sintering studies since the Pd atoms not only sinter, but also diffuse at a comparable or even faster rate through the oxide thin film and bind to the underlying NiAl.[13] Therefore, we have chosen to use the (0001) surface of bulk α-Al_2O_3 for this study. The insulating properties force use of an alternative microscopy that does not require a conducting sample, such as AFM. We operate the AFM in noncontact mode (frequency modulation[14]) since it is expected that in contact mode the AFM tip will move the Pd particles, as has been observed in STM experiments of Pd particles on graphite.[15]

Alumina is a common support for metal catalysts and, as a large band-gap insulator, is an ideal sample on which to test the capabilities of NC-AFM. The α-Al_2O_3 unit cell has hexagonally close packed layers of oxygen anions, with two layers of aluminum cations between each oxygen layer along the [0001] direction. The α-Al_2O_3(0001) surface is terminated by a single aluminum layer (half of the Al bilayer), but the terminating aluminum layer relaxes to be nearly coplanar with the underlying oxygen layer.[16,17] The surface structure has been studied with high-resolution transmission electron microscopy,[18] reflection electron microscopy,[19] and low-energy electron diffraction (LEED).[17,20–22]

Previous AFM studies of the α-alumina surface have shown that terrace size and step edge smoothness are affected by annealing at high temperatures in air.[23–26] Air-annealing maintains the α-Al_2O_3(0001)-(1×1) surface, while vacuum annealing at high temperatures leads to a variety of surface reconstructions, including a stable $(\sqrt{31}\times\sqrt{31})R\pm9°$ reconstruction.[27] These surface reconstructions can be reversed by annealing in an oxygen background.[20] Although we could routinely produce the $(\sqrt{31}\times\sqrt{31})R\pm9°$ reconstruction, all of the data shown in this paper are from the (1×1) surface.

In addition to the AFM work mentioned above, which showed terraces and steps of the alumina surface, atomic and near-atomic resolution of flat, clean oxide surfaces has been achieved by NC-AFM.[28–31] That work has shown atomically spaced features, such as surface atoms or unit cells. However, relatively little work has been done using NC-AFM to observe particles and clusters on the α-Al_2O_3(0001) surface. Furthermore, to our knowledge, only one AFM study of Pd clusters on this surface has been published,[32] although there is some AFM and transmission electron microscopy work on metals on MgO(100).[33–36] Other groups have used STM to study sintering of metal clusters on semiconducting oxides such as TiO_2(110) and ZnO.[37,38] Here, we have used NC-AFM to image Pd clusters sintered to different temperatures on the α-Al_2O_3(0001) surface.

Previous studies of Pd vapor deposition on alumina reported layer-by-layer growth using Auger electron spectroscopy[39] or three-dimensional (3D) island growth using secondary ion mass spectrometry,[40] x-ray photoelectron spectroscopy (XPS),[41] and NC-AFM.[32]

II. EXPERIMENT

LEIS and AFM experiments were done in two different ultrahigh vacuum (UHV) chambers, both with base pressures in the low 10^{-10} Torr range. For both types of experiments, single crystal α-Al_2O_3(0001) samples were obtained from SCI Engineered Materials, Inc. and Alfa Aesar. These were rinsed with methanol, then annealed in air (in a clean, closed alumina crucible) at 1670 K for 15–24 h. After annealing, the crystals were cleaned ultrasonically for 10 min several times in mild detergent, then in nanopure water, then in acetone, and finally in methanol.

The AFM experiments were done in an Omicron multiprobe surface science system (Omicron Nanotechnology GmbH) equipped with a variable temperature noncontact atomic force microscope. The AFM chamber is connected to a preparation chamber equipped with a Pd doser, an oxygen leak valve for annealing in O_2, and a water-cooled quartz crystal microbalance (QCM). The AFM chamber is also connected to an analysis chamber with XPS and LEED capabilities. For the NC-AFM experiments, sample heating to 1300 K was accomplished by resistive heating of a Ti/Pt film deposited on the back of the sample. Following the air anneal and ultrasonic cleaning, the crystals were coated on one side with 30 nm Ti (as an adhesion layer) and 120 nm Pt. Samples were cut by a diamond scribe and ground with a diamond grinding wheel to fit the Omicron AFM sample holder, then cleaned again ultrasonically in the solvents mentioned previously. Samples were cleaned *in situ* by annealing at 1000–1270 K in 5×10^{-7} Torr of O_2. Surfaces were cleaned until the XPS C 1*s* peak was below detection limits and NC-AFM showed atomically smooth, clean terraces. The analysis chamber is also equipped for Ar^+ sputtering. While sputtered and annealed surfaces showed a good LEED pattern, they had a higher density of steps with ragged edges and craters within the terraces, which made distinguishing particle structure from step structure difficult in AFM. Therefore, for each Pd dose reported here by AFM, a new alumina crystal was transferred into the chamber and prepared as above without any Ar^+ sputtering.

AFM images were recorded in UHV using the frequency modulation (noncontact) technique. The silicon AFM tips from Nanosensors™ are specified to have an end radius below 10 nm and are part of cantilevers with spring constants of about 42 N/m. The cantilevers have resonant frequencies in the range of 300–330 kHz and were operated at frequency shifts in the range -100–-50 Hz to obtain the images in this paper. Resonant frequency is measured by a beam deflection technique and although no direct measure of oscillation am-

plitude was made, we have calculated it to be about 10 nm. All NC-AFM images were taken at room temperature.

As alumina is a good electrical insulator, local surface charging can lead to poor image quality in NC-AFM due to long-range electrostatic forces between the tip and the sample. Compensation for these forces can be achieved by applying a bias between the AFM tip and the metal film on the back of the sample as has been similarly done for other insulating samples.[42] However, if the surface was highly charged (>6 V compensating voltage needed), applying a bias was less effective, and the images were generally of a lower quality. Bias voltage was chosen in the following manner. The tip position was held constant (no rastering or z feedback) and the frequency shift Δf was monitored as the bias on the tip, relative to the grounded metal film on the back of the sample, was ramped from -10 to $+10$ V. The magnitude of Δf typically had a well-defined minimum with respect to the applied bias. This minimum corresponds to the bias which most effectively compensates for the long-range electrostatic forces. This was done at different points during scanning and the bias voltage was set at the value for best images. However, ramping the bias in this manner sometimes made the tip unstable or changed the tip structure and so this procedure was avoided if a tip was imaging particularly well. In those cases, the ideal bias voltage for scanning was determined by changing the bias voltage slowly during scanning and using the value which gave the best images. The optimum bias voltage for good imaging varied widely from day to day with no systematic trend over the range of voltages available in our microscope (-10–$+10$ V), probably due to variations in the initial charge on the sample. The seven images shown in this paper were taken with bias voltages ranging from -3.9 to $+9.4$ V ($\sim+2$ V average and ~4 V standard deviation).

LEIS and TP-LEIS experiments were done in a separate chamber described in detail elsewhere,[43,44] which was also equipped for XPS, temperature-programmed desorption (TPD) and LEED. For these experiments, the sample was mounted in a Ta support attached to Ta wires for resistive heating. The samples were cleaned by Ar^+ sputtering (8×10^{-6} Torr Ar, 670 eV beam energy) between each experiment, then annealed at 1000 K in 5×10^{-5} Torr of O_2 for 30 min. Surface cleanliness was verified by XPS. Sputtering was necessary to remove Pd from the previous experiments in this chamber, because the sample holder in this chamber did not permit easy sample exchange as in the AFM system. This difference in surface preparation may lead to differences in Pd growth, which we assess below.

For both NC-AFM and LEIS experiments, Pd was dosed at room temperature from a homemade source (described previously[45]) consisting of Pd wire (Alfa Aesar, 99.997 % pure) wrapped around a resistively heated W filament. Dose rates, measured by QCM, were ~1 Å/min in the LEIS experiments and ~0.4 Å/min for the NC-AFM experiments. Coverages of Pd θ_{QCM}, were determined from this dose rate, and are reported in monolayers (ML). One ML is defined as the Pd(111) packing density, 1.5×10^{15} atoms/cm^2, which at palladium's bulk packing density corresponds to a ML thickness of 0.22 nm. For sintering studies by AFM, the Pd-covered surface was annealed at a given temperature for ~1 min, then allowed to cool to room temperature before imaging. TP-LEIS experiments used a heat ramp of 1 K/s. All LEIS was done using a defocused 500 eV He^+ ion beam at a He pressure of 5×10^{-8} Torr in the UHV chamber, which gave an ion current to the sample of about 0.1 μA. This led to drastic sample charging which seriously distorted the LEIS spectrum. The charging was effectively compensated to yield an excellent LEIS spectrum by using a defocused, 100 eV electron beam operated at a current to give zero net current to the sample.

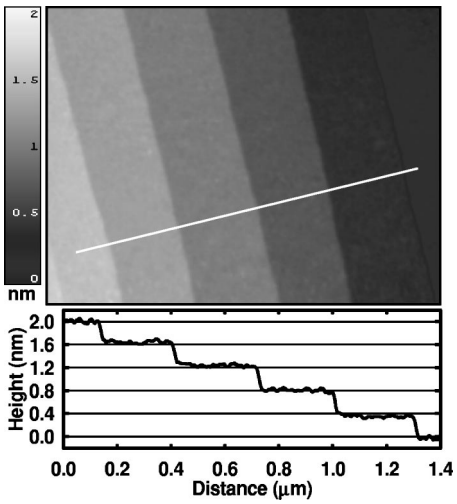

FIG. 1. 1500×1120 nm^2 (3.0 nm z range) NC-AFM image of clean, unreconstructed α-Al_2O_3(0001) surface. Line profile shown in lower panel is along the white line in the upper panel. The terraces are 250–300 nm wide and the steps are 0.4 nm high. Vertical z height represented by gray scale as indicated in the bar at left (same range as in profile); lighter shading represents high regions of the surface and darker shading corresponds to lower regions. Image has been smoothed using a 2D Gaussian filter with standard deviation 3.8 nm. (Scan conditions: $\Delta f=-60$ Hz, $f_0=318$ kHz).

III. RESULTS / DISCUSSION

A. Clean α-Al_2O_3(0001) surface

The cleaning and preparation procedure described above gives a clean and well-ordered (1×1) surface according to LEED, XPS, LEIS, and TPD. Figure 1 is a NC-AFM image of the clean alumina surface, showing atomically flat terraces 250–300 nm wide with step heights of 0.4 nm. Typically, samples prepared in this way have terraces 200–700 nm wide, and sharp step edges with heights in multiples of 0.2 nm. The most common step height we observed by NC-AFM was double step heights (0.4 nm), although we also observed 0.2 nm and 0.6 nm step heights. These step edges appear straight (within our resolution) typically for lengths of >300 nm. Earlier experimental work reported step heights of 0.22 nm (Ref. 24) and 0.2 nm (Refs. 25, 30, and 32) as well as step bunching which produced steps in heights of multiples of 0.2 nm.[24,26,46] The alumina (0001) surface is terminated by a layer of Al atoms, i.e., half of the Al atom bilayer. The periodicity of Al bilayers along the [0001] direction is 0.21 nm, which is one sixth of the unit cell. It has been proposed that the step heights measured by AFM reflect this spacing.[32,47] The step bunching which produces multiple

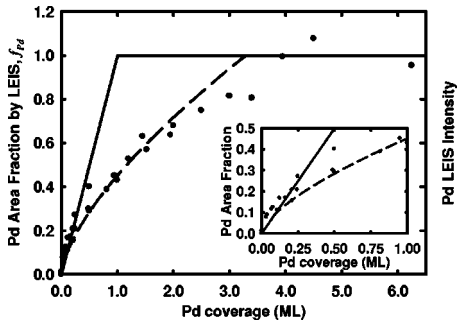

FIG. 2. Dots: The Pd LEIS intensity, extrapolated to 300 K from TP-LEIS data (see Fig. 3), vs Pd coverage dosed to the oxide surface at 300 K. Since the Pd LEIS intensity here is normalized to that of a continuous Pd film, it equals the fraction of the oxide area covered by Pd, f_{Pd}. Solid line: Result expected for layer-by-layer growth of Pd. Dashed line: best fit of $f=a\theta^{2/3}$ (growth of 3D particles of a fixed shape; $a=0.45$) to the data points in the coverage range 0–2.0 ML. The inset shows the coverage range 0–1.0 ML expanded in scale. The data show that Pd grows as 2D islands up to a coverage of ~0.25 ML, after which it grows as 3D particles.

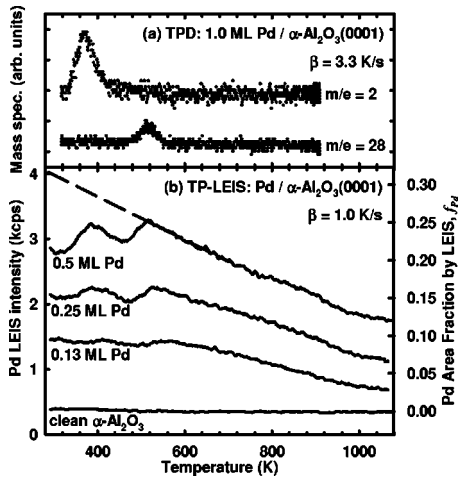

FIG. 3. (a) TPD (3.3 K/s) after dosing 1.0 ML Pd on α-Al_2O_3(0001). Peaks were seen at 370 and 520 K, attributed to H_2 ($m/e=2$) and CO ($m/e=28$), respectively, from H and CO adsorbed on the surface from the chamber background gas (mainly due to outgassing from the electron flood gun used for charge neutralization during TP-LEIS). (b) TP-LEIS (1 K/s) of different Pd coverages on α-Al_2O_3(0001). When H_2 and CO desorb from the Pd (as shown in top figure) at 350 and 490 K, the Pd LEIS signal grows. [A minor temperature decrease in desorption peak temperature arises from a decrease in heating rate (Ref. 51)]. The Pd signal decreases between the two desorption peaks with nearly the same slope as at higher temperature, and suggests that sintering is fast below 400 K and is significant at room temperature. Dashed line shows estimated TP-LEIS signal that would be seen if no H_2 and CO impurity were present.

layer step heights occur during the air anneal when heated above 1300 K.[24,26] It has been reported that shorter or lower temperature air anneals give smaller terraces with more single step heights and fewer multiple step heights[24] and we have found this to be true. For crystals which had a shorter anneal in the furnace than the others, we saw smaller terraces, 100–200 nm wide, with the majority of steps with 0.2 nm height. These surfaces also had more uneven step edges. Terraces of the clean alumina surface are flat (roughness less than peak-to-peak noise of 0.12 nm), but no atomic structure could be resolved, even though the typical rms average noise was less than 0.030 nm.

B. LEIS of the growth of Pd particles during Pd vapor deposition

We have monitored the growth of Pd on Al_2O_3(0001) by LEIS. Since LEIS is sensitive to only the top layer of the surface, we assume that the intensity of the Pd LEIS peak is proportional to the fraction of the alumina surface covered by Pd particles. In general, this has been a good assumption for other late transition metals on oxides such as ZnO, MgO, and TiO_2 whenever the metals cluster into islands.[45,48,49]

Figure 2 shows the fraction of the oxide surface area covered by Pd, as measured by LEIS, vs Pd dose θ_{QCM}. This fractional coverage of the oxide by Pd f_{Pd}, is simply the integrated intensity of the Pd LEIS peak (background corrected), normalized to that for a large dose that saturates this signal (>4 ML). (Here we also have corrected the LEIS signals obtained after dosing Pd at 300 K for an artifact due to adsorbed impurity CO and H by extrapolating the TP-LEIS signal after that Pd dose back down to 300 K, as described below when discussing Fig. 3.) The behavior of the Pd signal expected for layer-by-layer growth is represented in this figure by the solid black line with unit slope up to a Pd dose of 1 ML. The measured Pd signal initially follows this curve up to ~0.25 ML, after which it falls quickly below it. We interpret this as indicating that the Pd grows as 2D islands (1 atomic layer thick) up to a coverage of ~0.25 ML, after which they thicken and thus continue growing as 3D particles.

The dashed line in Fig. 2 represents a simplified 3D growth model. Here we have fit the data to the function $f=a\ \theta^{2/3}(a=0.45)$ in the coverage range 0.09–2 ML, which would occur if the particles kept the same 3D shape (e.g., hemispheres) and number density. (Note that this model is physically impossible below 0.09 ML, where it would predict islands less than one atom thick, i.e., $f>\theta$) This model underestimates f_{Pd} below 1 ML, and overestimates it above 2 ML, proving that the islands change shape with coverage, evolving from small thickness-to-width ratios to larger. The inset of Fig. 2 shows the coverage range 0–1.0 ML in expanded scale. In the range 0.1–0.25 ML, the LEIS data points are fitted better by the 2D model than the 3D model. The average relative magnitude of the deviations (i.e., the rms relative error) of the data from the model is 75% larger for the 3D fit compared to the 2D fit, where the rms error is only 19% and indistinguishable from the data scatter. Again, this indicates that the Pd grows as 2D islands (1 atomic layer thick) up to a coverage of ~0.25 ML. Note that the average island thickness in the 3D model increases between 0.1 and 0.25 ML from 1.0 to only 1.4 atomic layers, so this model is physically very similar to the 2D model in this coverage range, setting an upper bound on its error relative to that of the 2D model.

Cordatos *et al.*, using Auger electron spectroscopy (AES), have suggested layer-by-layer growth of Pd on this surface up to several monolayers.[39] Gillet *et al.*, using secondary ion mass spectrometry in static mode, have shown 3D clustering of Pd on the stoichiometric alumina surface

TABLE I. Summary of Pd particle average thickness, diameter, and number density for several Pd coverages and anneal temperatures. Thickness t_{LEIS} was derived from LEIS data for particle preparation conditions similar to those of the AFM images presented in this paper (see references in third column). Average apparent diameter measured by AFM, $\bar{d}_{AFM}$, as well as particle number density from AFM, N_{AFM}, are presented. The apparent Pd coverage $\theta_{AFM/LEIS}$ is calculated from t_{LEIS}, $\bar{d}_{AFM}$, and N_{AFM}, and the particle diameter estimate $d_{LEIS/AFM}$ is made from θ_{QCM}, t_{LEIS}, and N_{AFM}, as described in the text.

θ_{QCM} (ML)	T_{anneal} (K)	Figure	t_{LEIS} (nm)	$\bar{d}_{AFM}$[a] (nm)	N_{AFM}[b] ($10^{11}cm^{-2}$)	$\theta_{AFM/LEIS}$[c] (ML)	$d_{LEIS/AFM}$[d] (nm)
0.4	920	6(a)	0.60	7.4±1.7	8.0±0.3	0.94	4.8
0.8	300	4(b)	0.42	4.8±1.1[e]	22±10	0.76	4.9
0.8	680	4(c)	0.64	5.8±1.8[e]	18±6	1.4	4.4
0.8	930	6(b)	0.92	11.4±3.2	5.6±1.3	2.4	6.6
0.8	1000	4(d)	1.0	7.7±2.8[e]	11±2	2.4	4.5
0.8	930, 1000	6(b) and 4(d)[f]	0.97	9.6±3.5	8.8±3.3	2.8	5.1
2.0	750	[g]	1.0	7.8±1.6	19±1	4.2	5.4
2.0	1060	[g]	1.6	11.6±2.9	5.4±2.8	4.1	8.1

[a]Diameters of particles measured by line profile of AFM images. Many particles [see footnote [e]] were chosen at random from the image for measurement; average diameter and standard deviation of that set are shown. Standard deviation represents statistical error not systematic measurement error.
[b]Average and standard deviation of number densities from several consecutive AFM images recorded at different areas of the same sample.
[c]Coverage from AFM/LEIS calculated by assuming circular particles with diameter and number density measured by AFM and average thickness from LEIS.
[d]Diameter of particles assuming circular geometry, number density as measured by AFM, and average particle thickness measured by LEIS.
[e]These values of $\bar{d}_{AFM}$ represent averages over 60 particles selected at random from the indicated figures. Other rows are averages of 30 particles.
[f]Thickness t_{LEIS}, diameter $\bar{d}_{AFM}$, and number density N_{AFM} in this row are averages of previous two rows which have similar preparation conditions (0.8 ML annealed to ~1000 K).
[g]AFM images for 2.0 ML not shown as figures in this paper.

above ~0.4 ML and 2D clusters on the reduced surface.[40] Ricci *et al.* interpreted electron energy loss spectroscopy data as indicating 3D growth on stoichiometric alumina for all Pd coverages in their study, 0.23–1.8 ML.[50] Pang *et al.*, using NC-AFM, showed 3D clustering of Pd.[32] However, they could not image submonolayer coverages of Pd, so could not predict what the initial growth mode is. Our data show 2D island growth with the 2D to 3D island transition at ~0.25 ML. We note that the report of layer-by-layer growth used AES, the least surface-sensitive technique of those in these prior studies, so the fact that it missed these rather thin islands is understandable.

Our LEIS data directly provide the average Pd thickness within the Pd islands t_{LEIS}, given by the ratio of the Pd coverage divided by the Pd area fraction from LEIS: $t_{LEIS} = \theta_{QCM}/f_{Pd}$. Note that t_{LEIS} is the thickness the Pd would be if all islands were flat and of the same, uniform thickness. At ~1.2 ML Pd dose, for example, the surface is 50% covered by Pd (Fig. 2), giving an average particle thickness of 2.4 ML, or $t_{LEIS} = 0.53$ nm. At 4 ML, the islands have grown enough laterally to cover all of the alumina surface. Values of t_{LEIS} are listed in Table I for several Pd coverages and annealing conditions (corresponding to AFM experiments described below).

C. TP-LEIS of the sintering of Pd particles upon heating

We also monitored the sintering of the Pd particles as a function of temperature using TP-LEIS. In TP-LEIS, the Pd LEIS peak's maximum intensity is monitored as the temperature is ramped at fixed rate (1 K/s). As the Pd particles sinter into larger clusters, they cover less of the surface and the LEIS Pd peak intensity decreases. Figure 3(b) shows TP-LEIS sintering curves for several Pd coverages. In general, the Pd signal decreases as temperature increases at all starting coverages.

The transient increases in the Pd TP-LEIS signal at $T = 350$ and 490 K seen in all curves arise from recovery of the Pd signal as H_2 and CO desorb, as can be seen by comparison to the TPD spectra in Fig. 3(a). That is, immediately after dosing Pd at 300 K, some of the Pd LEIS intensity is masked by CO and H impurity adsorbed on the Pd islands from the background CO and H_2 in the chamber. The Pd signal recovers at 350 K and 490 K simultaneous with the desorption of H_2 and CO, respectively, as observed by TPD. (A minor temperature decrease in desorption peak temperature arises from a decrease in heating rate.[51]) The observed decrease in Pd TP-LEIS intensity between the CO and H_2 desorption temperatures, and even at temperatures below the H_2 desorption peak, suggests that sintering starts at temperatures below 400 K, and that there is significant sintering even at room temperature.

As noted above, we corrected the LEIS signal in Fig. 2 obtained after each Pd dose at 300 K for its decrease induced by these adsorbed impurities (CO and H). To determine what the LEIS signal would be for the clean, unsintered Pd islands at room temperature in the absence of this CO and H impurity, we used TP-LEIS data like in Fig. 3(b), and assumed a constant slope of the corrected TP-LEIS signal equal to its

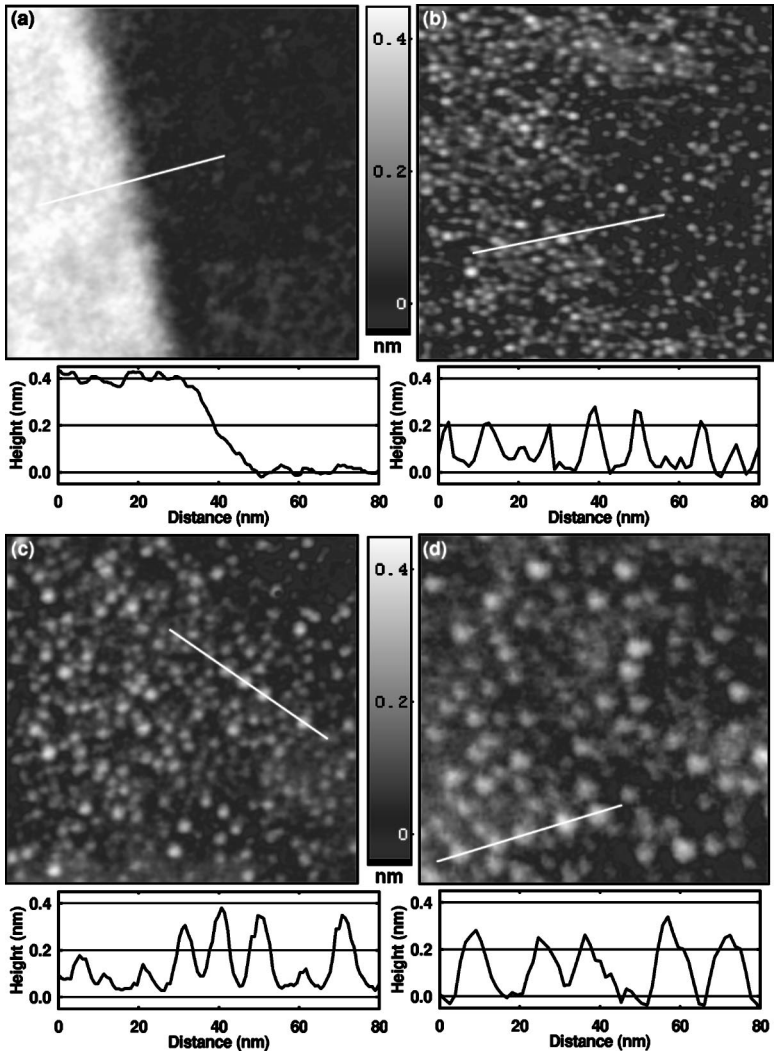

FIG. 4. 150×150 nm^2 (0.6 nm z range) NC-AFM images of (a) the clean alumina surface in an area containing one step and (b)–(d) 0.8 ML Pd in areas between step edges on the alumina surface. Pd particles shown (b) as dosed at room temperature, (c) after annealing to 680 K, and (d) after annealing to 1000 K. Before imaging (c) and (d), the sample was allowed to cool to room temperature. Height z represented by same gray scale in each panel. Paired with each image is a line profile taken along the white line indicated in the image. Some of the apparent roughness in (b) and (d) is due to pixelation. Images have pixel sizes of (a) 0.55 nm, (b) 1.3 nm, (c) 0.75 nm, and (d) 1.3 nm; each was smoothed with a 2D Gaussian filter of standard deviation 0.63 nm. [Scan conditions: (a) $\Delta f=-60$ Hz, $f_0=319$ kHz; (b) $\Delta f=-50$ Hz, $f_0=327$ kHz; (c) $\Delta f=-60$ Hz, $f_0=327$ kHz; and (d) $\Delta f=-79$ Hz, $f_0=327$ kHz].

slope in the long linear region just *after* CO desorption (i.e., from 550 to 750 K). Note that the slope between the H_2 and CO desorption peaks (i.e., from 380 to 460 K) is very similar to this slope above $T=530$ *K*, confirming this assumption. This slope was then linearly extrapolated back down to 300 K, as shown by the dashed line on the top TP-LEIS curve in Fig. 3(b). This corrected intensity was then normalized to the corrected signal for a saturation dose (i.e., 100% coverage of the oxide). For most of the coverages studied, the Pd clusters cover ~60% less surface area after ramping to 1000 K than they did at 300 K; i.e., the average thickness of the Pd particles more than doubles by 1000 K. No further sintering was observed by TP-LEIS for a Pd film that has already been annealed to 1000 K (not shown here).

From 400 K to 1000 K, the Pd LEIS signal decreases linearly with temperature, indicating a constant sintering rate (slope of Pd dispersion vs time) when probed at a constant heating rate. If we assume that during TP-LEIS the particles retain a fixed shape of either hemispheres or cylindrical disks of fixed thickness-to-diameter ratio, and a constant total volume of Pd, then the Pd particle diameter is inversely proportional to the Pd LEIS signal, and the number density of particles is proportional to the Pd LEIS signal cubed. Pd dispersion (the product of particle area times number density) is proportional to LEIS signal and decreases linearly with time.[11] Figure 3(b) shows that sintering causes the Pd particles to cover ~50% less of the alumina surface when heated from ~400 K to ~1000 K, which within these assumptions implies that they double in average thickness and diameter, and decrease by eightfold in number density. The assumption of constant volume below 1000 K is justified by the fact that Pd desorption from nanoparticles supported on a similar oxide (silica) does not start until above 1000 K.[52]

D. NC-AFM of Pd growth and sintering

Although LEIS techniques have the required surface sensitivity to measure the average Pd island thickness, they do not provide any information on the dimension of the particles in directions parallel to the surface, or their number density, nucleation sites, nor other local surface information. For this, we used noncontact AFM.

It should be noted that tip convolution effects in AFM can cause the apparent size of clusters to be distorted when the clusters are comparable in size to or smaller than the AFM tip (~10 nm end radius). The lateral dimensions of the particles are convoluted with the size and shape of the AFM probe tip. Long-range van der Waals forces between the tip and the substrate lead to an underestimation of the particle height for particles that are small relative to the size of the

AFM end radius, as will be discussed further in a future paper.[53] Inaccuracy in height measurements by AFM has been reported previously.[32,54,55] Hence in AFM images, Pd nanoparticles appear artificially wide and short.[56]

The growth and sintering of Pd particles was observed with AFM by imaging the clean alumina surface, and then imaging the surface after vapor deposition of Pd at room temperature and after several annealing treatments. Figure 4 shows a representative series of NC-AFM images of (a) the clean alumina surface, (b) after dosing 0.8 ML of Pd at room temperature, and after annealing to (c) 680 K and (d) 1000 K. Line profiles are shown for each image along the white lines shown. Each panel in Fig. 4 shows a 150 nm $\times$150 nm area taken from a larger image. We note that the images in panels 4(b)–4(d) were taken using the same sample surface (i.e., the same Pd dose) and the same Si AFM tip. This set allows for a more reliable comparison of particle size changes than one in which several AFM tips were used, although tip changes may have occurred between images that would distort relative comparison of particle sizes. Panel (a) shows the clean alumina surface near a step edge which is 0.4 nm high. After Pd deposition at room temperature (b) we observe Pd particles 4.8 ± 1.1 nm in diameter (baseline width average of 60 particles $\pm$ one standard deviation) and 2.8 ± 0.10 nm tall (maximum height of a hand-drawn curve through the middle of the noise), with a cluster density of 2.2×10^{12} clusters/cm^2 (obtained by averaging the cluster densities counted from multiple scans of different areas of the sample). Particle diameters reported in this paper were obtained from AFM line profiles through the centers of the particles, where the width is measured just high enough on the particle so as to be clearly discernible from the noise on the flat substrate. (For asymmetric particles, this was measured across the narrowest direction.)

Previous measurements of Pd island density for Pd deposited on a room temperature highly ordered Al_2O_3 thin film grown on NiAl(110) have found number densities of $\sim3\times10^{11}$ cm^{-2} for 0.8 ML Pd coverage by spot profile analysis SPA-LEED [SPA—spot profile analysis (Ref. 12)] and $\sim1\times10^{12}$ cm^{-2} for 1.5 ML Pd by STM.[57] The same STM study stated that the particle volume was about 3000 atoms, which corresponds to a diameter of about 2.8 nm for a hemispherical particle.[57] Clearly, the number densities are higher on α-Al_2O_3(0001), suggesting stronger adsorption or more defect sites.

After annealing to 680 K, the clusters have sintered and are larger, apparently 5.8 ± 1.8 nm wide, while the cluster density has decreased to 1.8×10^{12} cm^{-2}. Annealing to 1000 K, the trend continues: clusters are now apparently 7.7 ± 2.8 nm wide, while the cluster density decreased to 1.1×10^{12} cm^{-2}, half the cluster density of the unannealed surface. The magnitude of decrease in number density is not as dramatic as seen with TP-LEIS, probably due to the fact that AFM misses the smallest particles present at room temperature. Larger, fewer clusters at higher anneal temperatures suggest particle sintering, either by Ostwald ripening, wherein larger clusters grow at the expense of small ones, or particle diffusion and coalescence.[11]

To illustrate the evolution of the particles with annealing temperature, Fig. 5 shows a histogram of the particle diameters from Fig. 4(b)–4(d), compiled by selecting 60 particles at random from these figures and measuring their diameters as described above. Also shown are Gaussian functions representing the mean and standard deviation of each set. The distribution of particle sizes widens and shifts to larger diameters with increasing temperature.

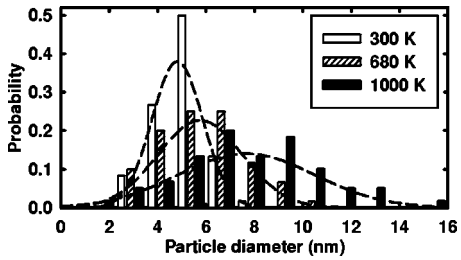

FIG. 5. Histogram of apparent Pd particle diameters for 0.8 ML Pd at room temperature (empty bars) and after annealing to 680 K (lined bars) and 1000 K (solid bars). These data were compiled from the images shown in Figs. 4(b)–4(d), respectively. The three data sets were taken on consecutive days using the same Si AFM tip on the same sample. The mean and standard deviation of each set (see Table I) were used to calculate the position and width of the three Gaussian curves shown as dashed lines.

It is likely that some of the smallest particles were missed in the cluster counting. By NC-AFM, we have observed clusters down to $\sim$2.5 nm in apparent diameter, but not smaller. At lower temperatures or lower Pd coverages, there are a higher fraction of small particles on the surface and so our estimates represent a lower limit of number density in those cases.

For coverages below 0.8 ML, it was difficult to image Pd as dosed at room temperature. Usually, annealing to higher temperatures was required before clusters on the surface could be seen by NC-AFM. There may be several explanations for this. Possibly, the Pd clusters are so mobile on the surface that they are pushed away by the AFM tip or blurred out by rapid atomic motion, or the Pd may be in the form of 2D islands with an apparent height less than the noise of the scan. The few images of unannealed Pd at 300 K that resolved clusters [e.g., Fig. 4(b)] were taken quite a long time after deposition ($>$1 h), during which sintering even at 300 K or background CO adsorption may have had an effect. (TP-LEIS showed that sintering starts below 400 K).

Figure 6 shows representative images collected over smaller areas and therefore with shorter pixel length [0.25 and 0.44 nm, respectively, compared to 1.3 nm in Figs. 4(b) and 4(d)] of two different Pd coverages, 0.4 and 0.8 ML, both annealed to $\sim$925 K. The particle densities for the two coverages are similar, 7.5×10^{11} cm^{-2} and 5.6×10^{11} cm^{-2}, respectively, but the higher Pd coverage surface has larger clusters: apparently 11.4 ± 3.2 nm in diameter compared to apparently 7.4 ± 1.7 nm in diameter for the lower Pd coverage surface.

Table I summarizes the average apparent diameters $\bar{d}_{\mathrm{AFM}}$ and number densities N_{AFM} of the Pd particles from these AFM images. Each number density is an average of several consecutive images at different areas on the same surface. For a constant coverage, it is observed that particle diameter increases and number density decreases with increasing an-

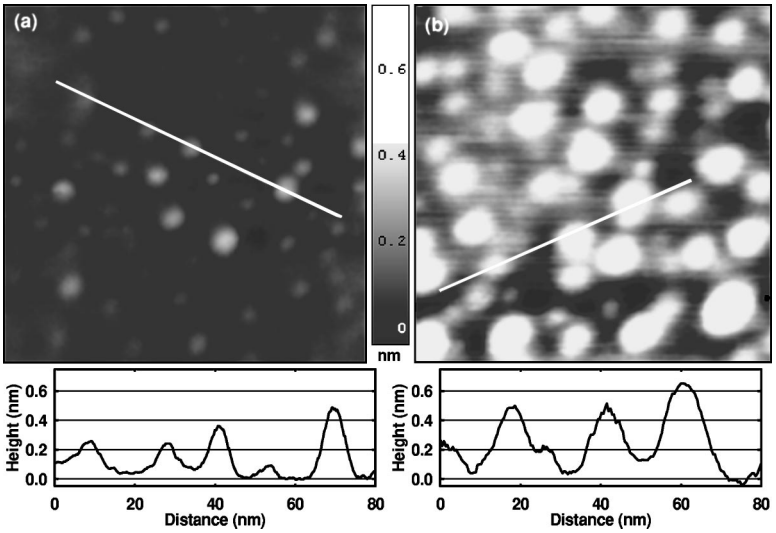

FIG. 6. 100×100 nm^2 (0.8 nm z range) NC-AFM images of (a) 0.4 ML and (b) 0.8 ML of Pd, dosed at 300 K and annealed briefly to 920 and 930 K, respectively. Line profiles along the white lines are shown below each image. The islands on the higher coverage surface are larger than those of the lower coverage, while the total particle density is similar at these two coverages, 7.5×10^{11} cm^{-2} in (a) and 5.6×10^{11} cm^{-2} in (b). Images have pixel sizes of (a) 0.25 nm and (b) 0.44 nm; each was smoothed with a 2D Gaussian filter of standard deviation 0.37 nm. [Scan conditions: (a) $\Delta f=-87$ Hz, $f_0=307$ kHz and (b) $\Delta f=-84$ Hz, $f_0=305$ kHz].

neal temperature. Comparing different coverages for the same anneal temperature (~715 K, ~925 K, and ~1030 K; all ±35 K) shows an increase in particle diameter and decrease in number density with increasing coverage.

Using the AFM data in Table I together with the LEIS measurements of average particle thickness discussed earlier, we can draw a number of conclusions about the systematic errors in measuring particle sizes with NC-AFM, and determine better estimates of the true particle dimensions. From f_{Pd}, given by the LEIS and TP-LEIS experiments for any given Pd coverage and anneal temperature, we can calculate the average Pd thickness within the Pd islands t_{LEIS} as described above: $t_{\mathrm{LEIS}}=\theta_{\mathrm{QCM}}/f_{\mathrm{Pd}}$. The values of t_{LEIS} are given in Table I. Even though t_{LEIS} represents the Pd thickness averaged over the Pd particle areas, it is consistently nearly twice the maximum height seen by AFM line profiles.[56] This large decrease in apparent thickness is consistent with the difficulty of seeing 2D Pd islands with AFM.

Using t_{LEIS} together with the average particle diameter $\bar{d}_{\mathrm{AFM}}$ and cluster density N_{AFM} measured by AFM, we can calculate an apparent Pd coverage, assuming the particles have a circular footprint of diameter $\bar{d}_{\mathrm{AFM}}$. These coverages are listed as $\theta_{\mathrm{AFM/LEIS}}$ in Table I. They are consistently larger than the true coverage θ_{QCM}, which is consistent with the footprint of the particles as seen by AFM being somewhat larger than reality, due to the tip convolution effects mentioned above.

Using the AFM cluster density N_{AFM}, and assuming the Pd islands have a circular footprint and have an area-averaged thickness equal to t_{LEIS}, we can calculate the average cluster diameter $d_{\mathrm{LEIS/AFM}}$, required to reproduce the known Pd coverage θ_{QCM}. These values, listed in Table I, are uniformly smaller than the apparent AFM diameters, due to tip convolution. Assuming that AFM sees all the particles, this calculation of $d_{\mathrm{LEIS/AFM}}$ is a much more accurate estimate of particle size than AFM-measured particle diameters because it has been calculated using number density from AFM and average island thickness from LEIS, thus avoiding tip convolution artifacts. However, not all the particles are seen when not annealed, causing $d_{\mathrm{LEIS/AFM}}$ to be overestimated at 300 K (see Table I). Trusting $d_{\mathrm{LEIS/AFM}}$ at 1000 K, and the TP-LEIS estimate that the average particle diameter increases twofold from 400 to 1000 K (for all coverages studied), we estimate that $d_{\mathrm{LEIS/AFM}}$ should really be ~2.5 nm at 300–400 K for 0.8 ML Pd.

Because the alumina surfaces were sputtered and annealed before all LEIS and TP-LEIS experiments discussed here, whereas new, unsputtered samples were used for all the AFM experiments discussed here, there may be some differences in the behavior of the Pd film on the two surfaces. One effect of sputtering may be more nucleation sites for the Pd clusters, which would result in higher cluster densities in the TP-LEIS experiments than in the AFM experiments. This, in turn, may mean that 3D growth starts at higher Pd coverages on the sputtered surface. The 2D to 3D growth transition, shown in Fig. 2 to occur at 0.25 ML of Pd, may happen at a lower coverage on the unsputtered surfaces of the AFM experiments and clusters on these surfaces would be, on average, larger than predicted by LEIS.

To test the effect of this sputtering used in preparing the LEIS surfaces, we measured the ratio of the areas of the Pd($3d_{3/2}$) peak to the Al($2p$) peak in XPS for nine coverages between 0.1 and 1.0 ML of Pd at 300 K for surfaces prepared in both ways. In this coverage range, this XPS ratio increased linearly with Pd coverage on both types of surfaces. The value of this XPS ratio divided by the Pd coverage was 3.6% larger, on average, for surfaces prepared using sputtering. This difference is so small that it suggests that the differences in particles size and number density were probably not very significant. Assuming hemispherical particles and the AFM result for the number density of particles of 2×10^{12} cm^{-2} for the unsputtered samples, this Pd XPS signal difference would correspond to an average particle radius that was between 9% and 20% smaller on the sputtered surface in this coverage range, and a number density of particles that was between 37% and 100% higher on the sputtered surfaces. We made this estimate using the analytical formula for XPS (or AES) signals from hemispherical particles derived by Diebold *et al.*,[58] and assuming a mean free path of 1.7 nm for the Pd photoelectrons at 913.4 eV kinetic energy and 2.2 nm for the Al photoelectrons at 1178.9 eV, based on values tabulated by Tanuma *et al.*[59]

IV. CONCLUSION

The combination of LEIS with NC-AFM provides a powerful approach to study the growth and sintering of Pd particles on α-Al_2O_3(0001), and presumably other metal nanoparticles on other insulating substrates. Annealing the clean alumina crystals to 1670 K in air resulted in a surface with flat terraces and smooth step edges of heights in multiples of 0.2 nm. TP-LEIS showed 3D cluster growth for Pd dosed at room temperature, with the 2D to 3D island transition at ~0.25 ML coverage. TP-LEIS monitoring of the change in Pd surface area with temperature showed that sintering starts below 400 K, and proceeds at a constant rate from ~400 K to 1000 K, when the surface is heated at a constant rate. By 1000 K, the Pd clusters cover ~50% less of the surface. NC-AFM showed fewer, larger clusters after heating from 300 to 1000 K, and provides estimates of the number density of clusters. For the same anneal temperature, particle diameter increases and number density decreases with increasing coverage above 0.4 ML. Comparing AFM with LEIS proves that particles less than 3 nm in diameter are easily missed in NC-AFM, which also slightly overestimates particle diameter.

ACKNOWLEDGMENTS

The authors would like to acknowledge the U.S. Department of Energy Office of Basic Energy Sciences Chemical Sciences Division and the M. J. Murdock Charitable Trust for support of this work. L.T.N. also thanks the NSF for an IGERT Nanotechnology fellowship. S.L.T. acknowledges support from the Joint Institute for Nanoscience funded by the Pacific Northwest National Laboratory (operated by Battelle for the U.S. Department of Energy) and the University of Washington.

[1] E. Garbowski, C. Feumi-Jantou, N. Mouaddib, and M. Primet, Appl. Catal., A **109**, 277 (1994).
[2] F. Ribeiro, M. Chow, and R. A. Dallabetta, J. Catal. **146**, 537 (1994).
[3] S. C. Su, J. N. Carstens, and A. T. Bell, J. Catal. **176**, 125 (1998).
[4] K. Fujimoto, F. Ribeiro, M. Avalos-Borja, and E. Iglesia, J. Catal. **179**, 431 (1998).
[5] J. N. Carstens, S. C. Su, and A. T. Bell, J. Catal. **176**, 136 (1998).
[6] F. Solymosi, A. Erdohelyi, J. Cserenyi, and A. Felvegi, J. Catal. **147**, 272 (1994).
[7] W. S. Epling and G. B. Hoflund, J. Catal. **182**, 5 (1999).
[8] S. H. Oh, P. J. Mitchell, and R. M. Siewert, J. Catal. **132**, 287 (1991).
[9] J. G. McCarty, Catal. Today **26**, 283 (1995).
[10] P. Salomonsson, S. Johansson, and B. Kasemo, Catal. Lett. **33**, 1 (1995).
[11] C. T. Campbell, S. C. Parker, and D. E. Starr, Science **298**, 811 (2002).
[12] M. Baumer and H.-J. Freund, Prog. Surf. Sci. **61**, 127 (1999).
[13] M. Heemeier, S. Stempel, S. K. Shaikhutdinov, J. Libuda, M. Baumer, R. J. Oldman, S. D. Jackson, and H.-J. Freund, Surf. Sci. **523**, 103 (2003).
[14] F. J. Giessibl, Rev. Mod. Phys. **75**, 949 (2003).
[15] A. Piednoir, E. Perrot, S. Granjeaud, A. Humbert, C. Chapon, and C. R. Henry, Surf. Sci. **391**, 19 (1997).
[16] C. Verdozzi, D. R. Jennison, P. A. Schultz, and M. P. Sears, Phys. Rev. Lett. **82**, 799 (1999).
[17] E. A. Soares, M. A. Van Hove, C. F. Walters, and K. F. McCarty, Phys. Rev. B **65**, 195405 (2002).
[18] L. A. Bursill, P.-J. Lin, and D. J. Smith, Ultramicroscopy **23**, 223 (1987).
[19] Y. Kim and T. Hsu, Surf. Sci. **258**, 131 (1991).
[20] T. M. French and G. A. Somorjai, J. Phys. Chem. **74**, 2489 (1970).
[21] C. C. Chang, J. Appl. Phys. **39**, 5570 (1968).
[22] P. S. P. Wei and A. W. Smith, J. Vac. Sci. Technol. **9**, 935 (1972).
[23] J. R. Heffelfinger, M. W. Bench, and C. B. Carter, Surf. Sci. **370**, L168 (1997).
[24] M. Yoshimoto, T. Maeda, T. Ohnishi *et al.*, Appl. Phys. Lett. **67**, 2615 (1995).
[25] A. Sasahara, H. Uetsuka, and H. Onishi, Jpn. J. Appl. Phys., Part 1 **39**, 3773 (2000).
[26] M. L. Hildner, T. J. Minvielle, and R. J. Wilson, Surf. Sci. **396**, 16 (1998).
[27] I. Vilfan, T. Deutsch, F. Lancon, and G. Renaud, Surf. Sci. **505**, L215 (2002).
[28] C. Barth and M. Reichling, Nature (London) **414**, 54 (2001).
[29] C. Barth and C. R. Henry, Phys. Rev. Lett. **91**, 196102 (2003).
[30] J. Wang, A. Howard, R. G. Egdell, J. B. Pethica, and J. S. Foord, Surf. Sci. **515**, 337 (2002).
[31] M. Ashino, Y. Sugawara, S. Morita, and M. Ishikawa, Phys. Rev. Lett. **86**, 4334 (2001).
[32] C. L. Pang, H. Raza, S. A. Haycock, and G. Thornton, Surf. Sci. **460**, L510 (2000).
[33] G. Haas, A. Menck, H. Brune, J. V. Barth, J. A. Venables, and K. Kern, Phys. Rev. B **61**, 11105 (2000).
[34] K. Hojrup-Hansen, S. Ferrero, and C. R. Henry, Appl. Surf. Sci. **226**, 167 (2004).
[35] H. Graoui, S. Giorgio, and C. R. Henry, Philos. Mag. B **81**, 1649 (2001).
[36] S. Giorgio, H. Graoui, C. Chapon, and C. R. Henry, Cryst. Res. Technol. **33**, 1061 (1998).
[37] M. Valden, X. Lai, and D. W. Goodman, Science **281**, 1647 (1998).
[38] L. V. Koplitz, O. Dulub, and U. Diebold, J. Phys. Chem. B **107**, 10583 (2003).
[39] H. Cordatos, T. Bunluesin, and R. J. Gorte, Surf. Sci. **323**, 219 (1995).
[40] E. Gillet, M. H. El Yakhloufi, J.-P. Disalvo, and F. Ben Abdelouahab, Surf. Sci. **419**, 216 (1999).
[41] V. Nehasil, S. Zafeiratos, V. Matolin, and S. Ladas, Vacuum **50**, 143 (1998).
[42] C. Barth and C. R. Henry, Nanotechnology **15**, 1264 (2004).
[43] K. H. Ernst, A. Ludviksson, R. Zhang, J. Yoshihara, and C. T. Campbell, Phys. Rev. B **47**, 13782 (1993).
[44] J. Yoshihara, J. M. Campbell, and C. T. Campbell, Surf. Sci. **406**, 235 (1998).
[45] A. W. Grant, L. T. Ngo, K. Stegelman, and C. T. Campbell, J. Phys. Chem. B **107**, 1180 (2003).
[46] L. P. Van, J. Cousty, and C. Lubin, Surf. Sci. **549**, 157 (2004).
[47] Z. Lodziana and J. K. Norskov, Surf. Sci. **518**, L577 (2002).
[48] C. T. Campbell, Surf. Sci. Rep. **27**, 1 (1997).
[49] S. Parker, A. W. Grant, V. A. Bondzie, and C. T. Campbell, Surf. Sci. **441**, 10 (1999).
[50] M. Ricci, B. Ealet, J.-M. Guglielmacci, and M. Gillet, Z. Phys. D: At., Mol. Clusters **26**, S67 (1993).
[51] P. A. Redhead, Vacuum **12**, 203 (1962).
[52] X. Xu, J. Szanyi, Q. Xu, and D. W. Goodman, Catal. Today **21**, 57 (1994).
[53] S. L. Tait, C. Polwarth, S. C. Fain, Jr., and C. T. Campbell (unpublished).
[54] F. J. Giessibl, Science **267**, 68 (1995).
[55] A. Sasahara, H. Uetsuka, T. Ishibashi, and H. Onishi, Appl. Surf. Sci. **188**, 265 (2002).
[56] S. L. Tait, L. T. Ngo, Q. Yu, S. C. Fain, Jr., and C. T. Campbell (unpublished).
[57] M. Frank and M. Baumer, Phys. Chem. Chem. Phys. **2**, 3723 (2000).
[58] U. Diebold, J.-M. Pan, and T. E. Madey, Phys. Rev. B **47**, 3868 (1993).
[59] S. Tanuma, C. J. Powell, and D. R. Penn, Surf. Interface Anal. **17**, 911 (1991).